J Mater Sci (2013) 48:7384–7391
DOI 10.1007/s10853-013-7553-9

Inhomogeneous softening during annealing of ultrafine-grained silver processed by HPT

Zoltán Hegedűs · Jenő Gubicza · Péter Szommer · Nguyen Q. Chinh · Yi Huang · Terence G. Langdon

Received: 6 June 2013 / Accepted: 24 June 2013 / Published online: 4 July 2013

Abstract The softening in ultrafine-grained silver processed by high-pressure torsion (HPT) was studied during annealing using differential scanning calorimetry (DSC). Two separate exothermic peaks were observed in the DSC thermogram of the HPT-processed sample. It is shown that the first and the second peaks are related to the recrystallization of the middle volume and the surface regions of the HPT-processed disk, respectively. Therefore, a very inhomogeneous sandwich-like microstructure develops during annealing with a soft interior and hard surface layers. The lower thermal stability of the middle region appears to be related to the stronger twinning activity since the twinned volumes can act as nuclei for recrystallized grains. The higher twin-fault probability in the interior is attributed to the larger strain due to the outflow of material between the anvils of the HPT facility during quasi-constrained processing.

Introduction

Contamination and porosity-free bulk ultrafine-grained (UFG) metals and alloys are often produced by severe plastic deformation (SPD). Two frequently used methods of SPD are equal-channel angular pressing (ECAP) [1–3] and high-pressure torsion (HPT) [4]. The stability of the UFG microstructures processed by SPD is a very important factor from the point of view of their practical applicability. The high-temperature thermal stability is often investigated by differential scanning calorimetry (DSC) [5, 6]. Usually a single exothermic peak is detected during the DSC scan which corresponds to recovery and recrystallization of the UFG microstructure. Although the temperature of the peak depends on the SPD-processing method, the imposed strain and the heating rate, its value is usually between ~ 0.3 and $0.4 \times T_m$, where T_m is the absolute melting point [7–10].

Among the face-centered cubic (fcc) metals and alloys processed by SPD, most of the DSC investigations were performed on materials with high or medium stacking fault energy (SFE) such as Al, Ni, and Cu [11–18]. However, it was shown earlier that the SFE has a significant effect on the thermal stability of UFG microstructures [19]. It seems that the rate of self-annealing in pure fcc metals increases with decreasing SFE [19]. This phenomenon means that the UFG microstructures processed by SPD at room temperature (RT) may exhibit recovery and recrystallization during their storage at RT. For example, self-annealing was observed in pure Cu and Ag samples [20–24]. However, due to its extremely low SFE (16–22 mJ/m^2 [25, 26]), the self-annealing in UFG Ag was faster than in Cu with the same impurity content [20–24]. In practice, the low SFE in Ag increases the inhomogeneity of the microstructure because low energy twin-faults can form at the expense of dislocations due to the stresses at glide obstacles [27–30]. Consequently, the recrystallization of this inhomogeneous microstructure is easier as the twinned volumes can act as nuclei in recrystallization [31].

Z. Hegedűs · J. Gubicza (✉) · P. Szommer · N. Q. Chinh
Department of Materials Physics, Eötvös Loránd University, Pázmány Péter s. 1/A, 1117 Budapest, Hungary
e-mail: gubicza@metal.elte.hu

Y. Huang · T. G. Langdon
Materials Research Group, Faculty of Engineering and the Environment, University of Southampton, Southampton SO17 1BJ, UK

T. G. Langdon
Departments of Aerospace & Mechanical Engineering and Materials Science, University of Southern California, Los Angeles, CA 90089-1453, USA

The method of SPD processing has an effect on the inhomogeneity of the UFG microstructure in silver. In a recent study [32] it was shown that a more inhomogeneous microstructure was formed in Ag during HPT than when processing by ECAP. The heterogeneity was most pronounced in the axial direction of the HPT disk. The middle of the sample processed by 1 revolution of HPT was coarse-grained with low hardness while the surface regions were hard with a grain size of about 200 nm. The interior of the disk may be recrystallized during its storage at RT before investigations. Axial heterogeneity of the microstructures formed by HPT was also observed for other materials, such as Cu [33] and an AZ31 Mg alloy [34–36]. Accordingly, this paper reports the inhomogeneity of softening in silver processed by 10 revolutions of HPT and annealed in DSC. The results show that the spatial variation of the thermal stability of the UFG microstructure may be correlated to the heterogeneity of the lattice defect structure in the axial direction of the HPT-processed disk.

Experimental materials and procedures

Silver of 99.99 % (4 N) purity was purchased from American Elements. This alloy was used in earlier studies [32, 37] and the alloying elements (in ppm) were documented by the supplier as Cu 30, Pb 10, Fe 10, Se 10, Sb 10, and Bi 20. Disks with diameters of 10 mm and thicknesses of about 0.8 mm were prepared and annealed at 741 K for 1 h before HPT processing. According to earlier investigations, the mean grain size of this initial material was $\sim$56 μm [32]. The annealed samples were deformed by HPT up to 10 turns. The applied load was 6.0 GPa and the processing was carried out at RT with a rotation rate of 1 rpm. The two anvils of the HPT device had shallow central depressions on their outer surfaces, with depths of 0.25 mm and diameters of 10 mm at the bottom and with slightly inclined walls having outer inclinations of 22°, as shown in an earlier report [32]. The thickness of the HPT-processed disks was $\sim$0.65 mm. All disks were processed under quasi-constrained conditions in which there is a small outflow of material between the two anvils during the processing operation [38, 39].

The microstructure after HPT was examined by X-ray line profile analysis (XLPA) at the half-radius of a disk as a function of the depth below the top surface. The time interval between HPT processing and XLPA measurements was 3 days due to the transportation of the samples. The measurements of the X-ray diffraction lines were performed using a special high-resolution diffractometer (Nonius FR591) with CuKα_1 radiation ($\lambda = 0.15406$ nm). The penetration depth of X-rays with this wavelength in Ag is $\sim$5 μm. In order to measure the variation of the microstructural parameters inside the disk, material was gradually removed from the top surface by mechanical polishing using an alumina suspension with a particle size of 1 μm. In one step of polishing the thickness of the removed layer was $\sim$100 μm. The microstructure was examined at the top surface and at depths of 110, 200, and 300 μm beneath the top surface, where the latter location corresponds to the middle of the disk. The time needed for XLPA measurement at each depth was 1 day. The line profiles were evaluated using the Convolutional Multiple Whole Profile (CMWP) fitting procedure. In this method, the diffraction pattern is fitted by the sum of a background spline and the convolution of the instrumental pattern and the theoretical line profiles related to the crystallite size, dislocations, and twin faults. The details of the CMWP procedure are available elsewhere [40, 41]. This method gives the crystallite size, the dislocation density, and the twin boundary probability with good statistics, where the twin boundary probability in fcc materials is defined as the relative fraction of twin boundaries among the {111} lattice planes.

In order to study the softening of the UFG microstructure obtained by HPT, an as-processed disk was annealed up to 650 K in DSC using a Perkin Elmer DSC2 calorimeter at a heating rate of 10 K/min. To examine the axial (perpendicular to the surface) inhomogeneity of softening, nanohardness maps were constructed on the cross section at the half-radius of the HPT-processed disk and also for the annealed samples which were heated up to the characteristic temperatures of the DSC thermogram at a rate of 10 K/min and then quenched to RT. The hardness measurements were carried out using a UMIS nanoindentation device with a Berkovich indenter and applying a maximum load of 5 mN. In each state a series of 400 indentations was recorded with the indents arranged in a 10 × 40 matrix with the distance of 15 μm between neighboring indents, as shown schematically in Fig. 1. The indentation measurements were started and finished at a distance of $\sim$25 μm from the top and bottom surfaces of the disk and forty indentations were made parallel to the axial direction which corresponds to the total thickness of the disk (650 μm). This process was repeated ten times, giving ten hardness values at each position along the axial direction. These values were then averaged and plotted as a function of the distance from the bottom of the disk.

The grain structure in the HPT processed and the subsequently heat-treated specimens was studied on the cross section at the half-radius of the disk by electron backscattered diffraction (EBSD) using a FEI Quanta 3D scanning electron microscope. First, the investigated surface was mechanically polished using an alumina suspension with the particle size of 1 μm. Then, a rectangular area of the surface with the dimensions of 100 × 100 μm^2 was

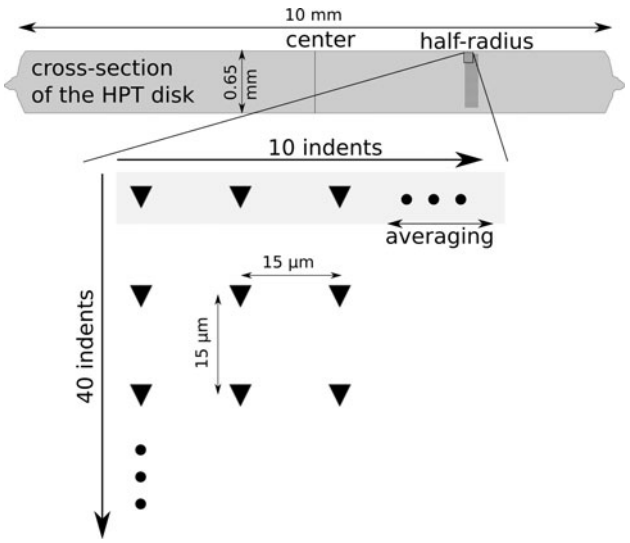

Fig. 1 Nanoindentation layout on the cross section of the HPT-processed disk

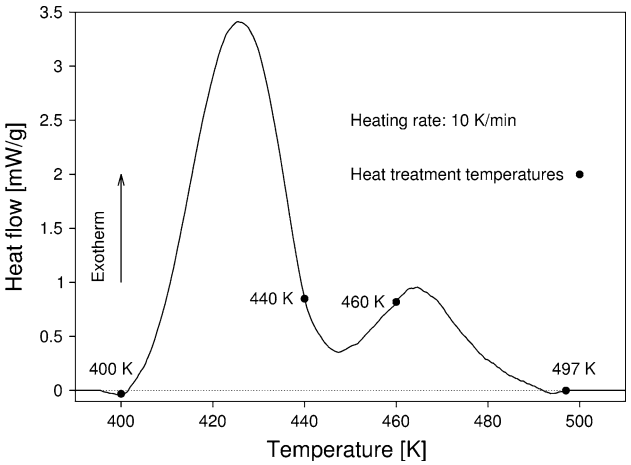

Fig. 2 DSC thermogram obtained at a heating rate of 10 K/min for the sample processed by 10 revolution of HPT. The temperatures of heat treatments are indicated by *solid circles*

etched by focused ion beam (FIB) of Ga^+ ions with an inclination angle of 3° using an accelerating voltage of 30 kV and an ion current of 15 nA. The finest step size in the EBSD experiments was set at 20 nm.

Experimental results

The DSC thermogram obtained on a silver disk processed by 10 revolutions of HPT is shown in Fig. 2. Two overlapping exothermic peaks were detected between 400 and 500 K, which correspond to the recovery and recrystallization of the UFG microstructure (see later). Without HPT processing there were no DSC peaks as the material was pure without any phase transformations. The first peak begins around 400 K and ends at 440–450 K, where the second peak begins. The end of the second peak is at ~497 K. In order to reveal the reason for the double DSC peaks, samples were heat treated up to the temperatures corresponding to the end of the first peak, as well as to the middle and the end of the second peak (440, 460, and 497 K, respectively) at a heating rate of 10 K/min.

The nanohardness distributions obtained on the cross sections of the HPT processed and the heat-treated disks are plotted as a function of the distance from the bottom surface in Fig. 3. It can be seen that after HPT the nanohardness distribution is homogeneous along the axial direction of the disk with a value of 1.8 ± 0.1 GPa. After annealing up to the first exothermic DSC peak, a relatively wide region of 250–300 µm in the middle of the disk shows a significant softening to a lower hardness value of 1.1 ± 0.1 GPa while the surface layers remain almost as hard as after HPT processing. There are clearly visible sharp transitions between the internal and surface regions. During the second exothermic peak (between 440 and 497 K), the surface regions of the disk also softened from about 1.8 GPa to 1.3 ± 0.1 GPa. However, the sharp transitions observed at 440 K disappeared at 460 K and instead the hardness increases almost linearly from the former transition layers to the surfaces. This result suggests that the softening of the surface region commences at the transition layers during the second exothermic peak.

The evolution of the grain structure during annealing of the HPT-processed disk was followed by EBSD on the cross section at the half radius. Figures 4a, b show EBSD images with an inverse pole figure at the top right of Fig. 4b where these images were obtained after the heat treatments performed up to 400 and 497 K, respectively.

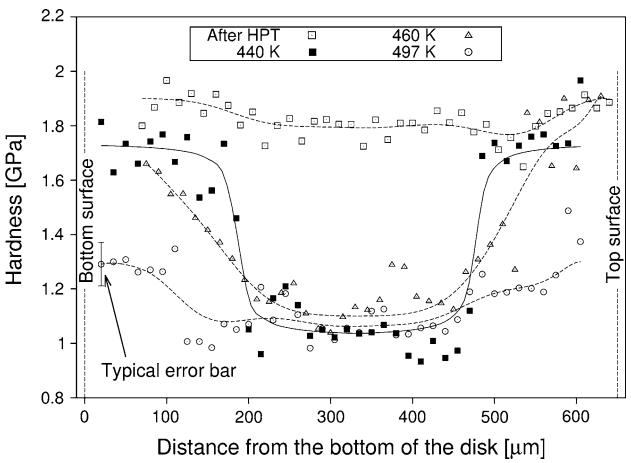

Fig. 3 Nanohardness distributions as a function of the distance from the bottom of the HPT-processed disk measured on the cross section in the axial direction. The *lines* serve only as guides to the distributions. The typical *error bar* is illustrated on the *left side* of the figure

The mean grain size was determined by averaging the equivalent circle diameters considering grain areas on EBSD images. At 400 K, the average grain size was ~170 nm throughout the sample if only the volumes with misorientations higher than 5° were considered as separate grains. When this misorientation limit was increased to 15°, the grain size value from EBSD evaluation increased to 200 nm. These values agree within the experimental error with those determined after HPT processing. After the second exothermic peak at 497 K, a fully recrystallized microstructure is observed throughout the disk with a characteristic grain size of ~50 μm. The recrystallized grains contain a large number of subgrains with a size of ~1 μm which are bounded by twin boundaries. The presence of these twinned volumes is explained by the very low twin boundary energy of silver (~8 mJ/m^2 [25, 26]).

Between the two exothermic peaks at about 440 K the nanohardness measurements showed a very narrow transition layer ~170 μm under both surfaces of the disk (see Fig. 3). The EBSD image in Fig. 4c was taken in this region after the heat treatment up to 440 K. The position of the transition layer is denoted by a dashed line. On the left side of Fig. 4c a part of a recrystallized grain with a size larger than the linear dimension of the image can be seen from the middle region of the disk. There are numerous small twin-oriented subgrains inside the large grain. The inset in Fig. 4c shows a higher magnification EBSD image of these fine subgrains taken from the designated square on the left of the dashed line. The right side of Fig. 4c corresponds to the surface region of the disk which remains as a UFG structure even after the heat treatment up to 440 K. The presence of a UFG structure is confirmed at the higher magnification in Fig. 4d. The average grain size values in the surface region at 440 K with misorientation limits of 5° and 15° were 165 and 180 nm, respectively.

In order to reveal whether any change took place in the surface region during the first exothermic peak, the grain size and the misorientation distributions in the surface layers were determined from the EBSD images at both 400 and 440 K and these results are plotted in Fig. 5. There is only a slight increase in the grain size and a negligible change in the misorientation distribution for the surface regions when the temperature increases from 400 to 440 K. The hardness and EBSD observations suggest that the first exothermic DSC peak is primarily caused by recovery and recrystallization in the middle of the disk, while the second peak corresponds to recovery and recrystallization of the

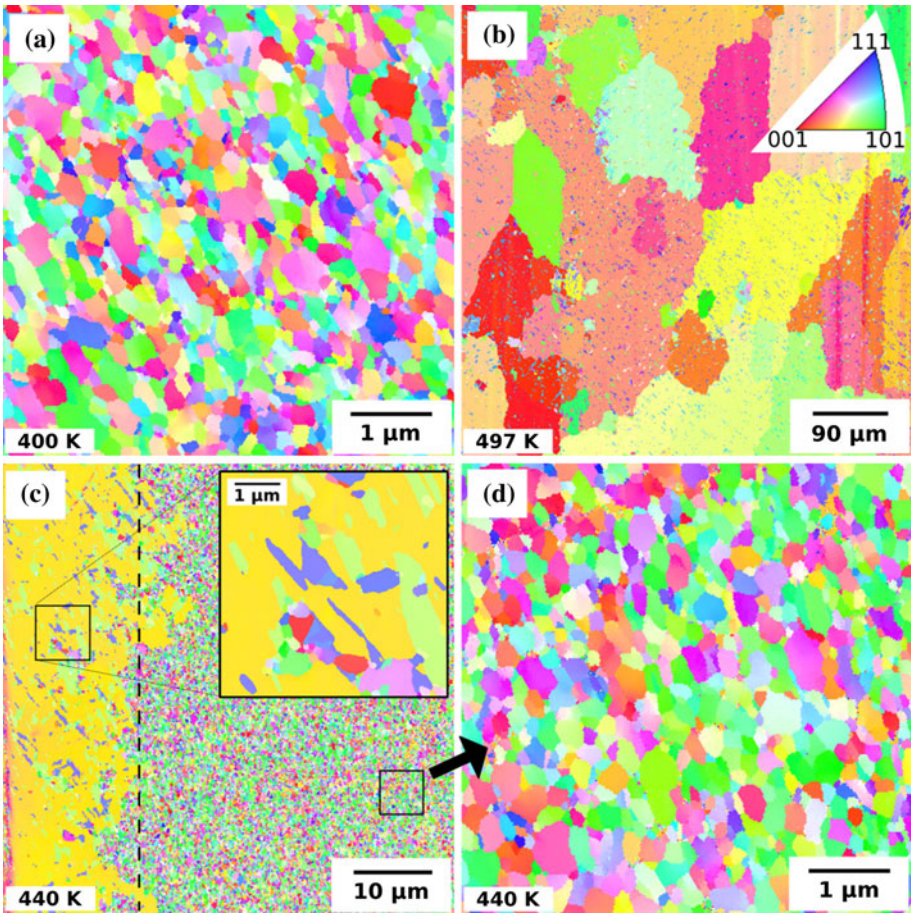

Fig. 4 EBSD micrographs showing the UFG microstructure before the exothermic DSC peaks at 400 K (**a**) and after the second peak at 497 K (**b**). The microstructure after the first DSC peak at 440 K is shown in (**c**) where the transition layer between the recrystallized interior and the UFG surface layer is indicated by a *dashed line*. The *inset* in (**c**) shows a part of the recrystallized grain in a higher magnification, illustrating that the large grain contains smaller twinned subgrains. A part of the UFG microstructure in the surface region is shown in a higher magnification in (**d**)

surface regions of the HPT-processed disk. These results demonstrate that the UFG microstructure in the interior of the disk processed by 10 revolutions of HPT is less stable than the surface regions, leading to an inhomogeneous softening during the heat treatment in DSC. According to the nanohardness measurements, the volumes of the disk interior and the surface regions are very similar, however the released heat during the DSC scan was significantly smaller for the second peak corresponding to the recovery and recrystallization of the surface regions. This dichotomy can be explained by the remaining UFG volumes in the surface regions at 497 K as suggested by their slightly higher hardness compared to the values determined for the middle of the disk (see Fig. 3). Direct evidence for this assumption was not obtained, since the preparation of the surface by FIB limited the area to 100 × 100 μm^2 investigated by EBSD. However, it was shown recently for the same material processed by 4 passes of ECAP that 17 % of the microstructure remained UFG even at high temperatures where no additional heat release was detected during annealing in DSC [37].

In order to reveal the reason for the gradient in the thermal stability in the axial direction of the HPT-processed disk, the characteristics of the microstructure were determined by XLPA as a function of the depth beneath the top surface. The crystallite size, the dislocation density, and the twin-fault probability are shown at different locations from the top surface to the mid-plane of the disk in Fig. 6. These results provide clear evidence for axial inhomogeneity of the lattice defect structure in the HPT-processed sample. The average crystallite size, the dislocation density, and the twin-fault probability were 56 ± 6 nm, 109 ± 11 × 10^{14} m^{-2}, and 0.9 ± 0.1 % at the top surface of the disk, respectively. In the surface layer with the thickness of 170 μm, the parameters of the microstructure did not change significantly. However, in the middle of the disk, at a distance of 300 μm from the surface, the dislocation density was lower (79 ± 9 × 10^{14} m^{-2}) while the crystallite size (80 ± 9 nm) and the twin-fault probability (1.6 ± 0.1 %) were larger than at the surface. Former studies [27–30] have shown that plastic straining of low SFE fcc metals such as Ag, lattice dislocations are dissociated into twinning partials at glide obstacles such as Lomer-Cottrell locks or grain boundaries and consequently twins may then form by slipping of these partials in neighboring {111} lattice planes. The stronger twinning activity in the interior of the sample is most probably a consequence of the geometry of the quasi-constrained HPT processing facility since in the middle of the sample the metal can flow outwards during SPD while in the surface regions the material is constrained by the walls of the HPT anvils. The larger plastic straining in the middle of the sample most probably results from an increase of the number of glide obstacles where twinning may occur due to the large stresses [42].

A former investigation [19] suggested that, in the volumes where the twin-fault probability increased at the expense of the dislocation density, the stored energy decreased due to the very low twin boundary energy of Ag. Thus, these volumes can act as nuclei for new defect-free grains during annealing, thereby reducing the time required for recrystallization in the middle of the HPT-processed Ag disk. The initiation of structural relaxation of the microstructure in the interior of the sample is also indicated by the larger crystallite size compared to the value determined in the surface region. It is noted that the crystallite size obtained by XLPA for metals processed by SPD is usually about 2–6 times smaller than the grain size determined by transmission electron microscopy (TEM) since the former

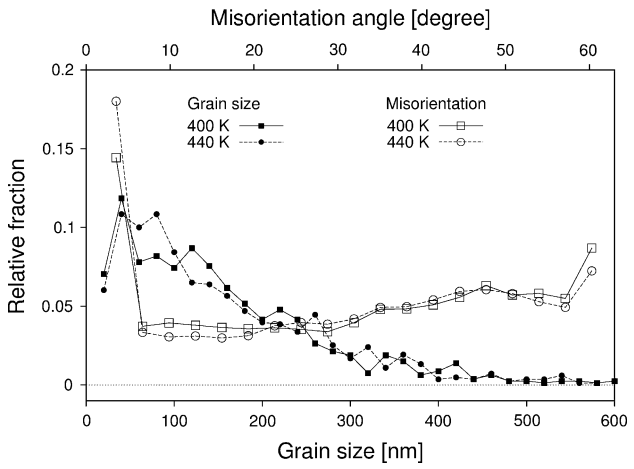

Fig. 5 Grain size and misorientation angle distributions in the surface region before and after the first DSC peak at 400 and 440 K, respectively, as obtained from the EBSD images in Fig. 4a, d. In the determination of the grain size distribution, the volumes with misorientations higher than 5° were considered as separate grains

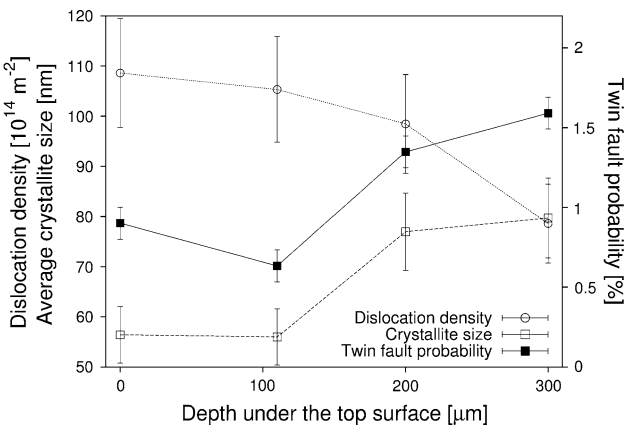

Fig. 6 The average crystallite size, the dislocation density, and the twin-fault probability determined by X-ray line profile analysis as a function of the depth beneath the top surface

quantity corresponds to the subgrain size [43]. Therefore, it is not necessary for the larger crystallite size in the middle of the disk to be accompanied by the larger grain size as obtained by EBSD. It should be noted that the nanohardness measurements and the microstructure investigations were performed only at the half-radius of the disk processed by 10 revolutions since previous studies have shown that the inhomogeneity in the hardness and microstructure in the radial direction is negligible even after 1 turn of HPT [32]. The lack of a considerable variation in the microstructure along the radial direction indicates a saturation in the vicinity of the center of the disk processed by 10 HPT revolutions.

Discussion

DSC scans for UFG fcc metals processed by SPD usually reveal only one exothermic peak in the thermograms. This peak corresponds to the recovery and recrystallization of the UFG microstructure. In the case of 99.998 and 99.99 % purity Ni samples processed by HPT at RT, two exothermic peaks were detected in the DSC thermograms [18, 44]. The first peak, appearing at a lower temperature of about 393 K at 10 K/min, corresponds to the disappearance of excess monovacancies while the larger second peak, at about 548 K, is associated with the annihilation of vacancy clusters and dislocations as well as recrystallization. The area under the first peak was about one order of magnitude smaller than for the second peak. The first "monovacancy" peak was not observed for 99.99 % Cu processed under the same conditions as most probably all the vacancies are clustered [44]. In the case of Ni, the high values of SFE and the high-melting point, together with the large pressures applied during HPT, retard the clustering of vacancies.

The single exothermic peak observed in the thermograms for the majority of SPD-processed UFG fcc metals indicates that the recovery and recrystallization occur at very close temperatures during DSC scans. However, when the UFG microstructure in Cu was obtained by the consolidation of powders using HPT technique, two exothermic peaks with similar areas were observed on the DSC thermogram [45]. The first and second peaks corresponded to the recovery and recrystallization of the microstructure, respectively. Both peaks appeared at higher temperatures than the single peak in the case of SPD-processed Cu. The more stable microstructure in the consolidated Cu sample is attributed to impurities and oxide dispersoids which are usually unavoidable in powder metallurgy. Thus, their pinning effect on grain boundaries is much stronger than on dislocations as suggested by the higher temperature of $\sim$250 K for recrystallization compared to recovery in the sintered specimen.

In the case of the present HPT-processed Ag sample, the double DSC peak is not associated with the very different temperatures of the recovery and recrystallization processes but rather it is due to the difference between the thermal stability of the UFG microstructures in the middle and the surface regions of the disk. The variation of the temperature of recovery and recrystallization in the axial direction is caused by the change of the lattice defect structure. In the whole sample, extremely high-dislocation densities (79–109 $\times$ 10^{14} m^{-2}) were measured by comparison with the saturation values obtained for other pure fcc metals processed by HPT [43, 46, 47]. The very high-dislocation density is attributed to the low SFE of silver, as the annihilation of dislocations is hindered by the high degree of dislocation dissociation. In low SFE metals such as Ag, twinning occurs at glide obstacles due to the large stresses [42].

In the middle of the disk the strain is larger than in the surface regions, as shown by model calculations [33], and this is due to the outflow of material between the anvils in quasi-constrained processing [48]. Therefore, in the interior of the disk it is anticipated that the number of glide obstacles is larger than in the surface regions, yielding larger twinning activity in accordance with the results of the present XLPA. An earlier study on ECAP-processed pure silver [19] showed that a larger twin-fault probability gave a weaker stability of the UFG microstructure against recrystallization. This effect is attributed to the very low energy of the twin boundaries. In the volumes where twin boundaries were formed at the expense of dislocations, the stored energy decreased locally by comparison with the neighboring regions. These volumes act as nuclei of defect-free new grains during subsequent annealing, thereby accelerating the recrystallization process. Therefore, in the middle of the disk where the twin fault probability is larger (1.3–1.6 $\pm$ 0.1 %) than in the surface regions (0.7–0.9 $\pm$ 0.1 %), the softening occurs at lower temperatures. Consequently, both the low SFE and the variation of the strain in the axial direction during HPT are necessary prerequisites for the observation of a double exothermic DSC peak. This is in accordance with the detection of a single DSC peak for pure Ag processed by ECAP [37]. It should be noted that inhomogeneities in the microstructure lead to easier recrystallization in any deformed metallic material [49]. Thus, for low SFE silver the difference in the stored energies in the twinned and dislocated volumes causes the inhomogeneity in the microstructure.

Axial heterogeneity in hardness and microstructure has already been observed for other HPT-processed materials, such as pure Cu [33], an Al–Mg–Sc solid solution [50], Mg-alloys [34–36], and the Zr_3Al intermetallic compound [51]. However, in the AZ31 Mg alloy and in Cu the observations show higher hardness in the vicinity of the

mid-plane of the sample and lower in the surface regions [33–36]. These studies explained this phenomenon in terms of the smaller grain size in the middle of the sample caused by the higher strain which is probably caused by the outflow of the material between the anvils. In the case of pure silver, the higher strain near the mid-plane of the HPT disk caused easier softening during subsequent heat treatment.

As in the present Ag sample, the transition layers between the middle and surface regions in the AZ31 alloy and the Zr_3Al intermetallic compound were also very thin [35, 51]. The reason for the sharpness of these layers is not clear at the present time and requires further investigation. Nevertheless, it should be noted that the microstructure changes only slightly along the radial direction of the Ag disk either immediately after 10 revolution of HPT or after subsequent annealing. This suggests there is an early saturation of the dislocation density due to their strong dissociation because of the low SFE.

In a recent study [32], the same Ag was processed by HPT for one revolution and showed a single exothermic peak during the DSC scan. The reason for the single exothermic peak is that the internal region of the sample processed by 1 turn was already recrystallized prior to the DSC experiment as confirmed by nanohardness measurements on the cross section. The thickness of this recrystallized volume and the hardness values of both the internal and surface regions in the disk deformed by 1 turn were very close to the values obtained for the present sample after the first exothermic peak at 440 K. Therefore, the single exothermic peak obtained for the sample processed by 1 turn corresponds to the recrystallization of the surface regions and therefore it is similar to the second peak detected in the present sample processed by 10 revolutions of HPT. The internal region of the sample processed by 1 turn may be recrystallized due to the increase of the temperature during HPT processing [39, 52] or due to transportation and storage before the investigation. An earlier study [19] showed that the UFG microstructures in SPD-processed Ag samples may recrystallize during their storage at RT. In the present sample deformed by 10 revolutions, the microstructure in the middle region remained UFG until the microstructural characterization which might may be due to a shorter storage period at RT.

Conclusions

1. The thermal stability of the UFG microstructure in Ag sample processed by 10 revolutions of HPT varied strongly in the axial direction of the disk. During annealing first the middle of the sample was softened while the surface regions remained as hard as immediately after HPT. The transition layer between the soft interior and the hard surface layers was very sharp, as revealed by nanoindentation. At higher temperatures, the surface regions of the disk were also recrystallized.

2. The spatially inhomogeneous thermal stability in the HPT-processed Ag specimen resulted in two separate exothermic DSC peaks: the first and second peaks were related to the recovery and recrystallization in the interior and the surface volumes of the disk, respectively. This behavior is unique among fcc metals and most probably can be attributed to the low SFE of Ag.

3. The easier recrystallization of the middle of the sample was most probably caused by the larger strain due to the outflow of the material between the anvils of the HPT facility. The higher straining in the interior yielded stronger twinning activity at the expense of dislocations, and these twinned volumes can act as nuclei in recrystallization.

Acknowledgements This study was supported in part by the Hungarian Scientific Research Fund, OTKA, Grant No. K-81360, the National Science Foundation of the United States under Grant No. DMR-1160966 (TGL), and the European Research Council under ERC Grant Agreement No. 267464-SPD-METALS (TGL). The authors thank Dr. Zoltán Dankházi, Dr. Károly Havancsák, and Mr. Gábor Varga for performing SEM/EBSD experiments.

References

1. Segal VM (1999) Mater Sci Eng A 271:322
2. Valiev RZ, Islamgaliev RK (2000) Alexandrov I V. Prog Mater Sci 45:103
3. Valiev RZ, Langdon TG (2006) Prog Mater Sci 51:881
4. Zhilyaev A, Langdon TG (2008) Prog Mater Sci 53:893
5. Molodova X, Gottstein G, Winning M, Hellmig R (2007) Mater Sci Eng A 460–461:204
6. Cao W, Gu C, Pereloma E, Davies C (2008) Mater Sci Eng A 492:74
7. Zhilyaev A, Nurislamova G (2002) Mater Phys Mech 5:23
8. Gubicza J, Dobatkin SV, Khosravi E, Kuznetsov AA, Lábár JL (2011) Mater Sci Eng A 528:1828
9. Gubicza J, Nam NH, Balogh L, Hellmig RJ, Stolyarov VV, Estrin Y, Ungár T (2004) J Alloy Compd 378:248
10. Gubicza J, Balogh L, Hellmig RJ, Estrin Y, Ungár T (2005) Mater Sci Eng A 400–401:334
11. Huang YK, Menovsky AA, De Boer FR (1993) Nanostruct Mater 2:587
12. Kumpmann A, Günther B, Kunze H-D (1993) Mater Sci Eng A 168:165
13. Zhilyaev A, Nurislamova G, Valiev R, Baro MD, Langdon TG (2002) Metall Mater Trans A 33:1865
14. Čížek J, Procházka I, Cieslar M, Kužel R, Kuriplach J, Chmelík F, Stulíková I, Bečvář F, Melikhova O (2002) Phys Rev B 65:094106
15. Zhilyaev AP, Gubicza J, Nurislamova G, Révész Á, Suriñach S, Baró MD, Ungár T (2003) Phys Status Solidi (a) 198:263
16. Zhilyaev A, Kim B, Szpunar J, Baro MD, Langdon TG (2005) Mater Sci Eng A 391:377
17. Lugo N, Llorca N, Suñol JJ, Cabrera JM (2010) J Mater Sci 45:2264. doi:10.1007/s10853-009-4139-7

18. Setman D, Kerber MB, Schafler E, Zehetbauer MJ (2009) Metall Mater Trans A 41:810
19. Gubicza J, Chinh NQ, Lábár JL, Hegedűs Z, Langdon TG (2010) Mater Sci Eng A 527:752
20. Mishin OV, Godfrey A (2008) Metall Mater Trans A 39A:2923
21. Wang G, Wu SD, Zuo L, Esling C, Wang ZG, Lib GY (2003) Mater Sci Eng A 346:83
22. Estrin Y, Isaev NV, Lubenets SV, Malykhin SV, Pugachov AT, Pustovalov VV, Reshetnyak EN, Fomenko VS, Fomenko LS, Shumilin SE, Janecek M, Hellmig RJ (2006) Acta Mater 54:5581
23. Günther B, Kumpmann A, Kunze H-D (1992) Scr Metall Mater 27:833
24. Gertsman VY, Birringer R (1994) Scr Metall Mater 30:577
25. Hirth JP, Lothe J (1982) Theory of dislocations. John Wiley and Sons Inc., New York
26. Murr LE (1975) Interfacial phenomena in metals and alloys. Addison Wesley, Reading
27. Venables JA (1961) Philos Mag 6:379
28. Cohen JB, Weertman J (1963) Acta Metall 11:996
29. Zhu YT, Liao XZ, Srinivasan SG, Lavernia EJ (2005) J App Phys 98:034319
30. Wang ZW, Wang YB, Liao XZ, Zhao YH, Lavernia EJ, Zhu YT, Horita Z, Langdon TG (2009) Scr Mater 60:52
31. Paul H, Driver JH, Maurice C, Piatkowski A (2007) Acta Mater 55:575
32. Hegedűs Z, Gubicza J, Kawasaki M, Chinh NQ, Lábár JL, Langdon TG (2013) J Mater Sci 48:4637. doi:10.1007/s10853-012-7124-5
33. Jeong HJ, Yoon EY, Lee DJ, Kim NJ, Lee S, Kim HS (2012) J Mater Sci 47:7828. doi:10.1007/s10853-012-6540-x
34. Figueiredo RB, Aguilar MTP, Cetlin PR, Langdon TG (2011) Metall Mater Trans A 42:3013
35. Figueiredo RB, Langdon TG (2011) Mater Sci Eng A 528:4500
36. Kawasaki M, Figueiredo RB, Langdon TG (2012) J Mater Sci 47:7719. doi:10.1007/s10853-012-6507-y
37. Hegedűs Z, Gubicza J, Kawasaki M, Chinh NQ, Süvegh K, Fogarassy ZS, Langdon TG (2013) J Mater Sci 48:1675. doi:10.1007/s10853-012-6926-9
38. Figueiredo RB, Cetlin PR, Langdon TG (2011) Mater Sci Eng A 528:8198
39. Figueiredo RB, Pereira PHR, Aguilar MTP, Cetlin PR, Langdon TG (2012) Acta Mater 60:3190
40. Ribárik G, Gubicza J, Ungár T (2004) Mater Sci Eng A 387–389:343
41. Balogh L, Ribárik G, Ungár T (2006) J Appl Phys 100:023512
42. Müllner P, Solenthaler C (1997) Mater Sci Eng A 230:107
43. Gubicza J (2012) Defect structure in nanomaterials. Woodhead Publishing Ltd., Cambridge
44. Setman D, Schafler E, Korznikova E, Zehetbauer M (2008) Mater Sci Eng A 493:116
45. Jenei P, Gubicza J, Yoon EY, Kim HS, Lábár JL (2013) Compos Appl Sci Manuf 51:71
46. Čížek J, Janeček M, Srba O, Kužel R, Barnovská Z, Procházka I, Dobatkin S (2011) Acta Mater 59:2322
47. Zhang HW, Huang X, Hansen N (2008) Acta Mater 56:5451
48. Song Y, Yoon EY, Lee DJ, Lee JH, Kim HS (2011) Mater Sci Eng A 528:4840
49. Ivasishin OM, Shevchenko SV, Vasiliev NL, Semiatin SL (2006) Mater Sci Eng A 433:216
50. Sakai G, Nakamura K, Horita Z, Langdon TG (2005) Mater Sci Eng A 406:268
51. Geist D, Rentenberger C, Karnthaler HP (2011) Acta Mater 59:4578
52. Edalati K, Miresmaeili R, Horita Z, Kanayamad H, Pippan R (2011) Mater Sci Eng A 528:7301